

Assessing Pair Interaction Potentials of Nanoparticles on Liquid Interfaces

Paul Y. Kim, Yige Gao, Yu Chai, Paul D. Ashby, Alexander E. Ribbe, David A. Hoagland, and Thomas P. Russell

ACS Nano, **Just Accepted Manuscript** • DOI: 10.1021/acsnano.8b08189 • Publication Date (Web): 13 Feb 2019

Downloaded from <http://pubs.acs.org> on February 15, 2019

Just Accepted

“Just Accepted” manuscripts have been peer-reviewed and accepted for publication. They are posted online prior to technical editing, formatting for publication and author proofing. The American Chemical Society provides “Just Accepted” as a service to the research community to expedite the dissemination of scientific material as soon as possible after acceptance. “Just Accepted” manuscripts appear in full in PDF format accompanied by an HTML abstract. “Just Accepted” manuscripts have been fully peer reviewed, but should not be considered the official version of record. They are citable by the Digital Object Identifier (DOI®). “Just Accepted” is an optional service offered to authors. Therefore, the “Just Accepted” Web site may not include all articles that will be published in the journal. After a manuscript is technically edited and formatted, it will be removed from the “Just Accepted” Web site and published as an ASAP article. Note that technical editing may introduce minor changes to the manuscript text and/or graphics which could affect content, and all legal disclaimers and ethical guidelines that apply to the journal pertain. ACS cannot be held responsible for errors or consequences arising from the use of information contained in these “Just Accepted” manuscripts.



1
2
3
4
5
6
7
8
9
10
11
12

Assessing Pair Interaction Potentials of Nanoparticles on Liquid Interfaces

13
14
15

AUTHOR NAMES

16 Paul Y. Kim¹, Yige Gao¹, Yu Chai^{2,3,4}, Paul D. Ashby³, Alexander E. Ribbe¹, David A.
17 Hoagland^{1*}, Thomas P. Russell^{1,2,5*}

18
19
20
21
22
23
24

AUTHOR ADDRESS

25 ¹ Department of Polymer Science and Engineering, University of Massachusetts Amherst,
26 Amherst, Massachusetts 01003, United States

27
28
29
30 ² Materials Sciences Division, Lawrence Berkeley National Laboratory, Berkeley, California
31 94720, United States

32
33
34 ³ Molecular Foundry, Lawrence Berkeley National Laboratory, Berkeley, California 94720, USA

35
36
37 ⁴ Department of Materials Science and Engineering, University of California, Berkeley,
38 Berkeley, California 94720, United States

39
40
41 ⁵ Beijing Advanced Innovation Center for Soft Matter Science and Engineering, Beijing
42 University of Chemical Technology, Beijing 100029, China
43
44
45
46
47
48
49
50
51
52
53
54
55
56
57
58
59
60

ABSTRACT

The pair interaction potentials of polymer-grafted silica nanoparticles (NPs) at liquid surfaces were determined by scanning electron microscopy, exploiting the nonvolatility of ionic liquids to stabilize the specimens against microscope vacuum. Even at near contact, individual, two-dimensionally well-dispersed NPs were resolved. The potential of mean force, reduced to the pair interaction potential for dilute NPs, was extracted with good accuracy from the radial distribution function as both NP diameter and grafted polymer chain length were varied. While NP polydispersity somewhat broadened the core repulsion, the pair potential well-approximated a hard sphere interaction, making these systems suitable for model studies of interfacially bound NPs. For short (5 kDa) poly(ethylene glycol) ligands, a weak ($<k_bT$) long-range attraction was discerned, and for ligands of identical length, pair potentials overlapped for NPs of different diameter; the attraction is suggested to arise from ligand-induced menisci. To understand better the interactions underlying the pair potential, NP surface-binding energies were measured by interfacial tensiometry, and NP contact angles were assessed by atomic force microscopy and transmission electron microscopy.

KEYWORDS

nanoparticles, polymer ligand, liquid interface, interaction potential, ionic liquid, electron microscopy, atomic force microscopy

1
2
3 Liquid interfaces are an important platform for nanoparticle (NP) assembly. Simply by their
4 preferential wetting, binding energies 10-1000 times thermal energy can effectively attach larger
5 (>10 nm) NPs to vapor-liquid or liquid-liquid interfaces without impeding NP lateral motions.¹
6
7 This combination of stability and mobility facilitates the convenient assembly of two-dimensional
8 (2D) NP arrays and crystals, which have many potential applications in materials science.² NP
9
10 interfacial systems also attract fundamental interest from the condensed matter community, as they
11 supply opportunities for model studies of 2D particle ordering in contexts ranging from
12 crystallization to vitrification/jamming.³⁻⁵ Compared to larger colloidal particles, the weaker
13 interactions between NPs lead to a faster approach to equilibrium and greater sensitivity/selectivity
14 to ligand-mediated NP-NP interaction potentials.

15
16
17 Understanding the in-plane interfacial interactions between NPs and developing strategies to
18 tailor these interactions are keys to controlling NP assembly at liquid interfaces. Usually, polymer
19 ligands are grafted to NPs to achieve stable 2D dispersion, borrowing a strategy better-known for
20 achieving 3D (or bulk) NP and colloid dispersion. The disposition of ligands when an NP is
21 partially wetted by two fluids is not well understood, but these ligands clearly influence the NP
22 contact angle.⁶ Among the governing variables are ligand length and stiffness, ligand grafting
23 density, and ligand interactions with the two surrounding fluids. Unlike larger particles, the
24 thickness of the ligand coating can exceed the particle diameter. Here, we disentangle some of
25 these complexities by using a recently-developed *in situ* scanning electron microscopy method
26 (SEM) to determine the equilibrium, in-plane NP pair interaction potential $U(r)$. To address the
27 physical interactions that underpin $U(r)$, companion microscopy methods were developed to
28 measure NP contact angle, and interfacial tensiometry was used to determine NP interface binding
29 energy.

1
2
3 Interactions between particles trapped at a liquid interface differ from those in a bulk liquid.^{1,}
4
5
6 ⁷ Particles at an interface are confined to a fluctuating surface separating phases that may differ in
7
8 density, solvation properties, ionic strength, and permittivity. The interface itself may host charges
9
10 or surface-active species that will affect van der Waals interactions as well as other solvent- and
11
12 interface-mediated interactions, for example, those created by a stabilizing ligand coating.⁸⁻¹⁰
13
14 Further, if the particles are charged and/or polarizable, in addition to the screened electrostatic
15
16 repulsions of the bulk, the symmetry breaking by the interface can produce strong dipole-dipole
17
18 interactions.¹¹⁻¹³ Even more, the menisci formed when the shapes of the particles are anisotropic,
19
20 uneven in contact line, or subject to external forces from buoyancy or electrostatic pressure create
21
22 strong capillary interactions.¹⁴⁻¹⁶ And, by perturbing capillary waves, particles display long-range
23
24 fluctuation-induced attractions.^{17, 18} In general, compared to micron-sized colloidal particles, the
25
26 interactions of NPs on an interface are weaker and shorter ranged, and with interfacial binding
27
28 energies also weaker, more sensitive to thermal fluctuations in areal density. Several investigators
29
30 reported that, tailored correctly, soft in-plane particle interactions can organize unusual 2D
31
32 phases,^{19, 20} motivating theories and microscopic models for NP interactions that go beyond
33
34 analogous theories and models for bulk interactions.

35
36
37
38
39
40 $U(r)$ captures the change in potential energy as two isolated, isotropic particles are brought
41
42 from infinity to finite separation r . $U(r)$ for colloidal particles in a bulk liquid have been measured
43
44 previously by atomic force microscopy,²¹ total internal reflection microscopy,²² surface forces
45
46 apparatus,²³ and optical tweezers.²⁴ Alternatively, $U(r)$ can be determined from the radial
47
48 distribution function $g(r)$, obtained by statistically analyzing the spatial arrangement of particles,
49
50 which connects to the potential of mean force $W(r)$ by $W(r)/k_b T = -\ln[g(r)]$, where k_b is the
51
52 Boltzmann constant, and T is the temperature.²⁵ Since $W(r)$ contains both binary and higher-body
53
54
55
56
57
58
59
60

1
2
3 interactions, extrapolating $g(r)$ to infinite dilution affords a straightforward path to $U(r)$.²⁶
4
5 Assessing interactions between NPs has been a great challenge since the typical imaging method,
6
7 optical microscopy, cannot be used with NPs due to the limited spatial resolution. Transmission
8
9 electron microscopy (TEM) has been used to obtain $U(r)$ for dispersed NPs in a bulk liquid;²⁷
10
11 however, due to the physical constraints of the liquid cell (*i.e.* ~ 100 -nm window gap and specimen-
12
13 window interactions), examination of liquid interfaces is compromised for TEM. Hence, NP
14
15 interactions on liquid interfaces have only been studied by computer simulations or *ex-situ*, after-
16
17 the-fact experimental observations.
18
19

20
21 In this study, using *in-situ* SEM to image particle positions, we sought $U(r)$ for ligand-coated
22
23 silica NPs on the surface of a nonvolatile, room temperature ionic liquid (IL) experimentally.
24
25 Experimental schematic and a typical SEM image are shown in Figure 1. We previously showed
26
27 that the selected SEM imaging protocol allows for high resolution investigations of NP structure
28
29 and dynamics, either in thin liquid films or on liquid surfaces.²⁸ At optimized imaging conditions,
30
31 features and positions below 5 nm can be resolved over interfacial areas containing hundreds to
32
33 thousands of NPs ($>300 \mu\text{m}^2$). With a large and diverse pool of anions and cations available, a
34
35 spectrum of IL physicochemical properties is readily accessed. While a few properties are distinct,
36
37 particularly nonvolatility and high ion conductivity, in most respects ILs are just solvents,
38
39 supporting the interactions typical of more traditional solvents such as hydrogen bonding,
40
41 Coulombic interactions, π - π interactions, and van der Waals interactions. Hence, ILs can serve as
42
43 model systems to probe interactions in liquids more generally. Here, NP diameter as well as ligand
44
45 molecular weight were varied to understand their influence on $U(r)$. To complement these
46
47 measurements and understand better the physical phenomena affecting $U(r)$, for the same NP-IL
48
49 combinations, the contact angle θ_c was determined by two microscopic methods, one based on
50
51
52
53
54
55
56
57
58
59
60

1
2
3 TEM and a second based on AFM. Lastly, to complete the fundamental characterization of the
4 system and verify the interfacial stability of the particles, NP interfacial binding energy was
5 determined by tensiometry.
6
7
8
9

10 11 12 RESULTS AND DISCUSSION 13

14 Supporting Information outlines the procedures followed for grafting 5 kDa and 40 kDa
15 polyethylene glycol (PEG) ligands onto 97 ± 9 , 202 ± 13 , 300 ± 14 nm spherical silica NPs, hereafter
16 referenced by their nominal 100, 200, and 300 nm diameters. For ligand attachment, bare silica
17 NPs purchased from Nanocomposix were aminated and then reacted with the succinimidyl ester
18 end groups of PEG ligands purchased from Sigma-Aldrich. The PEG grafting densities of the three
19 different sized NPs are summarized in Table 1. While not varying significantly with NP size, the
20 density for 5 kDa PEG was approximately five times greater than for 40 kDa PEG, reaching ~ 0.5
21 chains/nm² for the former and ~ 0.1 chains/nm² for the latter. It is noteworthy that neither of these
22 PEGs dissolved in the IL at room temperature, but instead, depending on PEG concentration,
23 precipitated as a semi-crystalline solid or gel; the PEGs did molecularly dissolve in the IL at
24 slightly elevated temperature.²⁹ For these reasons, and given the relatively low grafting densities,
25 the PEG ligand coatings should not be considered a flexible polymer “brush” on the NP surface.
26
27 Nevertheless, the PEG ligands stabilized bulk NPs in either methanol or IL, with no evidence of
28 aggregation in low concentration dispersions over many months; however, when NPs were
29 jammed for hours in or on IL, irreversible aggregation was noted upon decompression.
30
31 Unfortunately, the PEG conformation in the IL could not be characterized by light scattering due
32 to the small difference in refractive index between PEG and IL, 1.470 and 1.477, respectively. The
33
34
35
36
37
38
39
40
41
42
43
44
45
46
47
48
49
50
51
52
53
54
55
56
57
58
59
60

1
2
3 PEG ligands probably formed a disordered, slightly semi-crystalline surface layer of high enough
4 density to prevent NP aggregation, either in IL bulk or on IL surface.
5
6

7
8 The surface energy γ of PEG is lower than that of IL, 43 mJ/m² vs. 48 mJ/m², and this
9 difference makes NP accumulation at the IL surface energetically favorable.^{30, 31} For a NP-
10 containing IL droplet created at time zero in the tensiometer, Figure S2 shows the time variation
11 of γ . As NPs migrated to the surface, γ dropped from 48 mJ/m² to 46 mJ/m². The free energy
12 change ΔE for attachment of one NP to a liquid surface can be expressed $\Delta E = \Delta\gamma A/N_s$,³² where
13 $\Delta\gamma$ is the γ decrease due to attachment of N_s NPs, and A is the surface area. As determined by
14 SEM, the steady state NP areal fraction ϕ , given $\pi a^2 N_s/A$, where a is the NP radius, was 0.74.
15 Dividing $\Delta\gamma$ by $\phi/\pi a^2$, ΔE ranged from ~ 500 (100-nm NPs) to $\sim 5,000 k_B T$ (300-nm NPs), large
16 enough to anchor a NP to the surface almost irreversibly. Consistent with such large binding
17 energies, over numerous SEM imaging experiments, no bound NP was ever observed to detach.
18 For the large (~ 100 nm diameter) NPs examined, contact line tension makes a negligible
19 contribution to binding energy.³³
20
21
22
23
24
25
26
27
28
29
30
31
32
33
34

35
36 At 3kV beam voltage, adsorption of electrons by the IL limited SEM imaging to features either
37 exposed to vacuum or covered by less than ~ 15 nm of IL. The bright, erratically moving circles
38 imaged for individual NPs never closely approached each other, defining a minimum center-to-
39 center separation of about the NP diameter, as expected if NP-NP contacts were too deeply
40 submerged to visualize. This mostly submerged status for NPs was confirmed by the θ_c
41 measurements. Figure 2 shows TEM and AFM measurements of θ_c for 5 kDa PEGylated NPs.
42 From the interface arrangement near the three-phase contact line, the TEM micrograph in Figure
43 2a for a 100-nm NP indicates that θ_c is $\sim 14^\circ$. For a small isotropic particle attached to a planar
44 liquid interface, a meniscus is typically not anticipated unless the particle surface is
45
46
47
48
49
50
51
52
53
54
55
56
57
58
59
60

1
2
3 inhomogeneous (see later discussion for amplification). TEM demonstrated that these NPs were
4 not perfectly smooth to the nanoscale, but by SEM of their exposed caps on the IL surface were
5 nearly circular, confirming close conformance (deviation to less than $\sim 3\text{-}5\text{ nm}$) to spherical shape.
6
7 Consistent with the uniformity in the NP surface and shape for both tested diameters and PEG
8 lengths, the TEM method illustrated in Figure 2 yielded a narrow range of θ_c , $12^\circ \lesssim \theta_c \lesssim 15^\circ$.
9
10 Clearly, the PEG ligands make the NPs highly IL solvophilic, as expected for the pairing of a polar
11 polymer with a polar liquid. At $\theta_c=14^\circ$, by simple geometry the horizontal mid-plane of a 100-nm
12 NP lies 48 nm below the IL surface, and further, the diameter of its vacuum-exposed spherical cap,
13 24 nm, is consistent with the size of (but smaller than) the bright circles in SEM images. (Each
14 circle includes, in addition to exposed cap, a ring of IL-submerged surface.)
15
16
17
18
19
20
21
22
23
24
25

26 For specimens dispersed or swollen by IL, imaging artifacts of TEM can be more serious than
27 those for SEM, mainly because oxidation-reduction chemistries are better triggered at the higher
28 electron energies of TEM. As noted previously, these chemistries cause IL viscosification and
29 eventual gelation (manifested as diminished motion of dispersed NPs).^{28, 34, 35} The “liquid” surface
30 shown in Figure 2a is actually the surface of a beam-solidified liquid, and during the solidification,
31 alterations to interface geometry/wetting could have occurred. An independent, confirming
32 measurement of θ_c was thus imperative. Figure 2b shows an AFM phase contrast image of mixed
33 100-nm and 200-nm NPs pinned to a silicon wafer by a surrounding IL film of thickness less than
34 either NP diameter. Air-IL-NP contact lines are clearly visible around individual NPs, verifying
35 that $\theta_c \ll 90^\circ$ (*i.e.*, a contact line below the NP mid-plane would be obscured). The contact line in
36 AFM appears as a boundary between the soft (dark) IL and the hard NP (bright) phases. Figure
37 2c plots the corresponding AFM height profiles along lines traced through NP apices (exemplified
38 for 200 and 100-nm NPs by arrows 1 and 2, respectively), and θ_c determined in this manner ranged
39
40
41
42
43
44
45
46
47
48
49
50
51
52
53
54
55
56
57
58
59
60

1
2
3 from 12° to 15°. Interestingly, θ_c around the periphery of the 200-nm NP labeled by arrow 2 varied
4
5 across a similar range. Contact line pinning on local defects (both chemical and topological) would
6
7 cause θ_c variations, and AFM probing of liquid height near a contact line may be imperfect.
8
9 Nevertheless, the close agreement between TEM and AFM determinations strongly supports the
10
11 accuracy of both methods and shows that, across the NP diameters, PEG chain lengths, and PEG
12
13 grafting densities examined, θ_c was essentially constant: a significant difference in NP-ligand
14
15 morphology has no discernable impact on θ_c .
16
17
18

19
20 Although SEM for ILs is less prone to imaging artifacts than TEM, pursuit of $U(r)$ by SEM
21
22 presents its own potential pitfalls. Incident electrons could affect the nominal values of $U(r)$
23
24 through mechanisms of electrostatic charging and/or heating, producing effects that scale with
25
26 electron dose.³⁶ For example, NP and IL surfaces might charge differentially, creating NP-NP
27
28 electrostatic interactions. To suppress such effects, specimens were imaged at a minimal electron
29
30 dose (~ 0.3 pC/ μm^2), and each area was imaged only once. Making certain that charging and
31
32 heating were negligible, $g(r)$ was measured for separate regions of the same specimen under
33
34 different magnifications: $\times 8000$, corresponding to a dose of 0.34 pC/ μm^2 (black curve), and $\times 6500$,
35
36 corresponding to a dose of 0.23 pC/ μm^2 (red curve). As seen in Figure 3a, the inferred $g(r)$ is
37
38 nearly identical, demonstrating that NP spatial arrangements were unperturbed at these low
39
40 electron doses. Fortunately, they were high enough to achieve adequate NP resolution. At higher
41
42 doses, imaging artifacts were identified, included directed NP motions, although the underlying
43
44 cause(s) were unclear. Literature suggests that electron conduction in ILs can mitigate charging
45
46 effects in SEM.^{28, 37}
47
48
49
50

51
52 Inversion of $g(r)$ yields the potential of mean force $W(r)$, a function dependent on ϕ (or
53
54 equivalently, areal number density). To determine $U(r)$, $W(r)$ can be extrapolated to zero ϕ , a route
55
56
57
58
59
60

1
2
3 previously pursued in optical microscopy studies of larger colloidal particles.²⁶ Figure 3b shows
4
5 $W(r)$ for NPs measured at ϕ equal to 0.018, 0.048, and 0.101 (areal number density equal to 0.58,
6
7 1.54, 3.22 NPs/ μm^2 , respectively) for 5 kDa PEGylated 200-nm NPs. $W(r)$ was essentially the
8
9 same at all ϕ , although because of the fewer NP pairs imaged, confidence in this conclusion at the
10
11 lowest ϕ is lower. $W(r)$ was also measured at $\phi = 0.29, 0.42, 0.57,$ and $0.65,$ equivalent to areal
12
13 number densities 14.5, 20.4, 27.1, and 30.9 NPs/ μm^2 , respectively, as shown in Figure S3. A
14
15 superposition of many body interactions produced stronger (and additional) peaks at higher ϕ . All
16
17 samples employed to determine $U(r)$ were sufficiently dilute to establish that $W(r) \approx U(r)$.
18
19
20

21
22 With NPs mostly immersed in IL, NP-NP interactions are anticipated to be dominated by
23
24 submerged close contacts between surface regions located around NP horizontal midplanes;
25
26 therefore, one might expect that NP-NP surface interaction resemble those in bulk IL. A bulk
27
28 Derjaguin-Landau-Verwey-Overbeek (DLVO) theory predicted that bare silica NPs aggregate in
29
30 a variety of imidazolium-based ILs,^{38, 39} consistent with our inability to disperse bare NPs either
31
32 in, or on, the IL. In the theory, strong screening by IL ions weakens the electrostatic repulsions
33
34 between NPs that would otherwise exist due their charge. This conclusion is challenged by recent
35
36 force measurements suggesting that electrostatic screening lengths in ILs are relatively large.^{40, 41}
37
38 Here, the PEG grafts reduced surface charge (converting a fraction of surface silanol group into
39
40 amide groups)⁴² and created a steric barrier beyond the range of bare surface van der Waals
41
42 attractions, factors favoring stability. Van der Waals attractions between NPs were diminished
43
44 further by the near match of NP, IL, and PEG refractive indices. Putting these considerations
45
46 together, NP-NP surface interactions would be anticipated to manifest dominantly PEG-PEG bulk
47
48 interactions, which unfortunately, proved difficult to characterize because refractive index
49
50 similarities thwarted light scattering experiments to probe bulk interactions. Assuming that the
51
52
53
54
55
56
57
58
59
60

1
2
3 PEG conformations were comparable to those at theta condition, the radius of gyration of 5 and
4
5 40 kDa PEG are ~ 6 and ~ 16 nm, respectively.⁴³
6

7
8 Figures 4a and b, focused on a dependence of $U(r)/k_B T$, plot this parameter against $r/2a$ for
9
10 100-, 200- and 300-nm NPs grafted with 5 kDa and 40 kDa PEG, respectively. For $r/2a$
11
12 approaching unity, *i.e.*, NPs approaching contact, the two plots reveal that $U(r)/k_B T$ is essentially
13
14 independent of a at constant PEG length. Just as striking, across the tested range, $1 < r/2a < 4$, the
15
16 magnitude of $U(r)/k_B T$ never exceeded 0.5, showing that NP-NP interactions were consistently
17
18 weak. The slight variation with a observed as $r/2a$ approaches unity is mostly an artifact of NP
19
20 size polydispersity, which created a distribution in closest NP-NP approach; in the abscissa of
21
22 these plots, " a " is the average of a distribution and not the value specific to an interacting NP pair.
23
24 The TEM-determined size polydispersities of 100-, 200- and 300-nm NPs, presented as the
25
26 coefficient of variation CV ($= s/a \times 100$, where s is the standard deviation in radius), were 9%, 6%
27
28 and 5%, respectively. At these levels, polydispersity can explain not only the a dependence
29
30 inferred at low $r/2a$ (less than ~ 1.3) but also why the downward jump in $U(r)/k_B T$ is not abrupt.
31
32 Supporting the latter argument, this jump is most abrupt for the sample of smallest polydispersity
33
34 (*i.e.*, largest a). These polydispersity arguments are buttressed in Figure S4, where a Gaussian
35
36 distribution of NP sizes was assumed and $g(r)$ then calculated as for hard spheres. The anticipated
37
38 broadening of core repulsions with polydispersity is observed. The experimental repulsion is
39
40 shifted slightly outward compared to the calculated one due to the latter's failure to account for
41
42 ligands. The magnitudes of the shifts are consistent with radii increases comparable to ligand size.
43
44
45
46
47
48

49 For $1.3 < r/2a < 2.3$, $U(r)/k_B T$ is negative for 5 kDa PEGylated NPs, reaching a minimum of
50
51 $\sim -0.19 k_B T$ at $r/2a = 1.6$, but across the same range $U(r)/k_B T$ for 40 kDa PEGylated NPs appears
52
53 slightly positive. Figure 4c compares the two behaviors for 200-nm NPs and clarifies the shape of
54
55
56
57
58
59
60

1
2
3 the broad $U(r)$ minimum for the shorter PEG ligand. The surface-to-surface separation at the
4 minimum is roughly equal to a for all three NP sizes, and the magnitude of the energy at this
5 position, while small, is almost an order-of-magnitude beyond the experimental error in $U(r)/k_bT$.
6
7 These surface-to-surface separations (50 to 150 nm) are much more than twice the root-mean-
8 square radius of gyration of the PEG chain at its theta condition (~ 12 nm) and, in two cases, much
9 more than twice the contour length (~ 70 nm).
10
11
12
13
14
15
16

17 These comparisons, and the lack of a comparable attraction for 40 kDa PEGylated NPs at any
18 separation, convincingly argue that, while PEG ligands are crucial, PEG-PEG solution interactions
19 are not the immediate source of the attraction. Instead, the large range of the attraction suggests a
20 capillary interaction as the source. We argue that, because of their lower surface energy, many
21 PEG ligands stretch in the IL to maximize their contact with the IL surface. Due to the stretching,
22 these chains exert, through their bound and adsorbed ends, a net upward force on the NP that is
23 equal and opposite to a spatially distributed force exerted downward on the IL surface. A result
24 of the forces will be a low amplitude meniscus around each NP. This ligand effect is distinct from
25 the localized impact of ligands on contact angle. Indeed, the greatest portion of the large NP
26 interfacial binding energy is attributed to PEG segments adsorbing to the IL surface. Absence of
27 the attraction for the 40 kDa PEG is most likely due to its lower NP grafting density reducing the
28 forces applied through ligands. For larger colloidal particles, because ligand size is insignificant
29 relative to particle size, all ligand impacts on the liquid surface can be subsumed into an altered
30 contact angle. We are unaware of theories or simulations able to predict how molecular weight
31 and grafting density affect the spatial disposition of flexible ligand segments around a liquid
32 interface-bound NP. Modeling is complicated by need to account not just for ligand stretching but
33 also grafting density, interfacial tensions (both ligand and liquid), and segment-segment
34
35
36
37
38
39
40
41
42
43
44
45
46
47
48
49
50
51
52
53
54
55
56
57
58
59
60

1
2
3 interactions near the no longer planar surface. Despite this complexity, similar weak attractions
4
5 would seem possible for all NPs drawn to a liquid surface by low surface energy polymeric ligands.
6
7 Others have proposed ligand-induced NP-NP interfacial attractions based on similar physical
8
9 depictions.⁴⁴⁻⁴⁷
10

11
12 To confirm the arguments of the preceding paragraph, the postulated meniscus would have to
13
14 be observed and quantified, a difficult experimental challenge since the meniscus deflection
15
16 immediately adjacent to the NP will be small, perhaps no more than a nanometer. Alternative
17
18 explanations for the attraction are elusive. Direct pairwise interactions between silica, PEG, or IL
19
20 can mostly be discounted due to the PEG molecular weight influence and the attraction's long
21
22 range, which is well beyond those of typical chemical interactions. Long range electrostatic
23
24 interactions are anticipated to be fully screened in these systems by the high density of free ions in
25
26 the IL. Lastly, capillary interactions due to particle roughness seem unlikely, although not fully
27
28 discounted, due to the uniformity of the attraction and its dependence on PEG molecular weight.
29
30
31
32
33
34

35 CONCLUSIONS

36
37
38 Pair interaction potentials between PEG-coated silica NPs attached to IL surfaces were
39
40 characterized by SEM imaging, exploiting the non-volatility of ILs. Artifacts arising from
41
42 exposure to the electron beam were characterized and found minimal at low electron doses. From
43
44 the measured radial distribution function, the potential of mean force was determined, and by
45
46 measurements at different but low particle densities, equivalence between this potential and the
47
48 pair interaction potential was established. The effects of particle diameter and grafted polymer
49
50 length on the potential were examined, and at constant length of grafted polymer, interactions were
51
52 insensitive to particle size. A weak long-range attraction (significantly less than the thermal energy)
53
54
55
56
57
58
59
60

1
2
3 was found for a short PEG ligand, and this attraction was explained in terms of a NP meniscus
4 induced by ligand interactions with the IL surface. Polydispersity in nanoparticle size broadened
5 the short-range repulsion caused by volume exclusion. The overall potential well conformed to a
6 hard sphere interaction, suggesting that the described NP-IL pairing is well-suited to serve as a
7 model system in studies of 2D particle packing and dynamics.
8
9
10
11
12
13

14 15 16 17 METHODS

18
19
20 **Grafting Density Measurement.** Grafting density was determined by thermogravimetric
21 analysis (TGA) of the solid produced when a methanol dispersion of the PEGylated NPs (5 mg in
22 50 μL) was dried in a furnace at 120°C for 2 h. After drying, weight loss was monitored during
23 10°C/min heating to 700°C (TA Instruments TGA Q50). Assuming PEG decomposition
24 accounted for the loss, grafting density was derived from the number of chains corresponding to
25 the weight lost divided by the particle surface area estimated from the weight remaining.
26
27
28
29
30
31
32
33

34
35 **SEM Specimen Preparation.** To minimize specimen charging during SEM imaging,
36 supports for IL were prepared by cutting conductive P-type silicon wafers (boron-doped, 0.001-
37 0.005 $\Omega\cdot\text{cm}$, Silicon Prime Wafers) into 1 cm squares that were etched for 15 min in a UV-ozone
38 cleaner. On a cut and cleaned square, a 3 μL IL sessile drop was deposited, and onto this drop,
39 1.5 μL of a diluted methanol NP dispersion was spread. The IL was 1-ethyl-3-methylimidazolium
40 ethylsulfate ([EMIM][EtSO₄], 99% purity), purchased from Iolitec and used without purification.
41 Since methanol and IL are miscible, the NP dispersion partially mixed during the introduction of
42 the IL, but as the methanol evaporated (a few minutes), the NPs segregated to the IL surface.
43 Before SEM examination, specimens were equilibrated in vacuum for 1 h to remove any residual
44 methanol or water (the IL is hygroscopic) and to allow the NPs to equilibrate in their 2D positions.
45
46
47
48
49
50
51
52
53
54
55
56
57
58
59
60

1
2
3 From the order of magnitude of the measured 2D interfacial NP diffusion coefficient at infinite
4 dilution, $D_o \sim 0.01 \mu\text{m}^2/\text{s}$, of the most sluggish 300-nm NPs, and supposing an NP areal density at
5 which the typical interparticle spacing is $\sim 1 \mu\text{m}$, the characteristic 2D equilibration time is $\sim 30 \text{ s}$.
6
7
8
9

10
11 **Imaging NP spatial distributions with SEM.** A SEM microscope (FEI Magellan XHR 400
12 FE-SEM) operated at 3 kV acceleration voltage and 50 pA beam current provided 1536×1024
13 pixel images of nominal $10 \times 10 \text{ nm}$ pixel size. To resolve two NPs in near contact while visualizing
14 dozens to hundreds of dilute NPs in the same frame, magnification was chosen such that NP
15 diameter corresponded to ~ 12 pixels and scan speed was adjusted to set the electron dose to ~ 0.3
16 $\text{pC}/\mu\text{m}^2$; electron dose was calculated as a number of incident electrons, *i.e.* beam current
17 multiplied by capturing time, per unit specimen area. For each specimen, 100 to 200 images were
18 collected at several surface locations, providing relative positional data for 30,000 to 50,000 NPs
19 in total. While the NPs retained unchanged surface mobility throughout imaging, reflecting the
20 absence of beam damage, the IL viscosity (122 cP) was large enough to keep the range of NP
21 Brownian motion insignificant compared to NP diameter over the 1~2 s image collection period.
22
23
24
25
26
27
28
29
30
31
32
33
34
35

36
37 **Calculation of $g(r)$ in 2D.** Images were filtered with a 4-pixel square Gaussian blur to reduce
38 noise and converted into binary images by intensity thresholding. Neighboring NPs artificially
39 fused by the binarization were separated by applying a modified watershed algorithm.⁴⁸ NP
40 position was assigned to the intensity centroid of the NP, and the 2D $g(r)$ was computed as the
41 number density of NPs at center-to-center separation between r to $r + dr$ normalized by the average
42 NP number density.
43
44
45
46
47
48
49
50
51

52 **Interfacial Tension Measurement.** NP interfacial activity was measured by pendant drop
53 tensiometry for samples prepared as just described except that the vacuum removal of
54
55
56
57
58
59
60

1
2
3 methanol/water was extended to two days. Water absorption during the measurements was
4
5 precluded by sealing the samples in nitrogen-purged cuvettes. Equilibration for ~24 h was
6
7 necessary to register a stable surface tension, reflecting the high IL viscosity and the diffusion-
8
9 controlled attachment of NPs to the interface. A stable surface tension signaled NP saturation of
10
11 the surface, with the NP areal fraction much greater than was employed in the measurement of NP
12
13 interactions. The difference in time scale between equilibration in 2D (*i.e.*, in the surface plane)
14
15 and 3D (*i.e.* during adsorption from the bulk), ~30 s vs. ~24 h, opened an intermediate time window
16
17 in which surfaces with NPs in their 2D equilibrated state could be studied by SEM reliably and
18
19 reproducibly at low areal density.
20
21
22
23

24
25 **Contact Angle Measurements by TEM and AFM.** IL nonvolatility facilitated two
26
27 unconventional microscopy methods for measuring θ_c . In the first, an IL dispersion of PEGylated
28
29 NPs was prepared as described above, and this dispersion was spread across a lacey carbon TEM
30
31 grid, removing any excess liquid by blotting with filter paper. Free-standing IL thin films of
32
33 nominal thickness less than either the grid thickness (~30-100 nm) or the NP diameter (≥ 100 nm)
34
35 were thereby created in grid openings. Due to pinning of the IL to the grid, the thicknesses of
36
37 these films were greater at their edges than at their middle, creating capillary forces on the NPs
38
39 that induced their migration to the edges.²⁸ At times much beyond those necessary for this
40
41 migration (seconds), the films ruptured due to capillary instability (the polar IL better wetted the
42
43 polar PEGylated NPs than the nonpolar carbon-coated grids), and most of the unpinned IL beaded
44
45 up, leaving many NPs attached at the grid opening edges by residual IL. Viewed by TEM (Jeol
46
47 2000FX) in profile, the residual liquid formed a three-phase contact line on the NP surface, and θ_c
48
49 was determined from the geometry imaged near this line. Analogous θ_c determinations were
50
51 described previously for larger particles imaged by optical microscopy.⁴⁹
52
53
54
55
56
57
58
59
60

1
2
3 In the second scheme, θ_c was extracted from the height profile of an NP and its surrounding
4 liquid for NPs pinned against a flat substrate by an IL volume too small to cover the NPs fully.
5
6 This geometry was created by spreading a dilute drop of NP-containing IL over a silicon wafer to
7 isolate substrate-trapped NPs. The NP apices were then height-profiled by AFM (Asylum Research
8 Cypher ES), and the air-IL-NP three phase contact point determined by fitting the NP portion of
9 the profile to a circle of NP diameter and the adjacent IL surface to a line of constant slope.
10
11 Schematics of the two contact angle measurements are shown in Figure S1. The TEM and AFM
12 measurements were conducted in vacuum and atmosphere, respectively.
13
14
15
16
17
18
19
20
21
22
23
24
25

26 ASSOCIATED CONTENT

27 28 29 **Supporting Information:**

30
31 Text outlining procedures for the grafting of PEG ligands to silica NPs; schematics of NP
32 wetting; time-dependent interfacial energy during NP adsorption; $g(r)$ and $W(r)$ at higher areal
33 number density; $U(r)$ model calculation for size-polydisperse NPs.
34
35
36
37
38
39

40 AUTHOR INFORMATION

41 42 **Corresponding Authors**

43
44
45 * Thomas P. Russell, E-mail: russell@mail.pse.umass.edu.

46
47 * David A. Hoagland, Email: hoagland@mail.pse.umass.edu.
48
49
50
51

52 ACKNOWLEDGMENTS

53
54
55
56
57
58
59
60

1
2
3 We acknowledge the financial support of the National Science Foundation through DMR-1807255.
4
5 The University of Massachusetts Materials Science and Engineering Center (MRSEC DMR-
6
7 0820506) partially funded P.Y.K.. Contact angle measurements by atomic force microscopy were
8
9 supported by the U.S. Department of Energy, Office of Science, Office of Basic Energy Sciences,
10
11 Materials Sciences and Engineering Division under Contract No. DE-AC02-05-CH11231 within
12
13 the Adaptive Interfacial Assemblies Towards Structuring Liquids program (KCTR16) and the
14
15 Molecular Foundry user program.
16
17
18
19
20
21

22 **Table 1. Grafting Densities of PEG on Silica NPs (chains/nm²)**
23
24

	100 nm	200 nm	300 nm
PEG 5 kDa	0.45	0.56	0.64
PEG 40 kDa	0.11	0.09	0.11

25
26
27
28
29
30
31
32
33
34
35
36
37
38
39
40
41
42
43
44
45
46
47
48
49
50
51
52
53
54
55
56
57
58
59
60

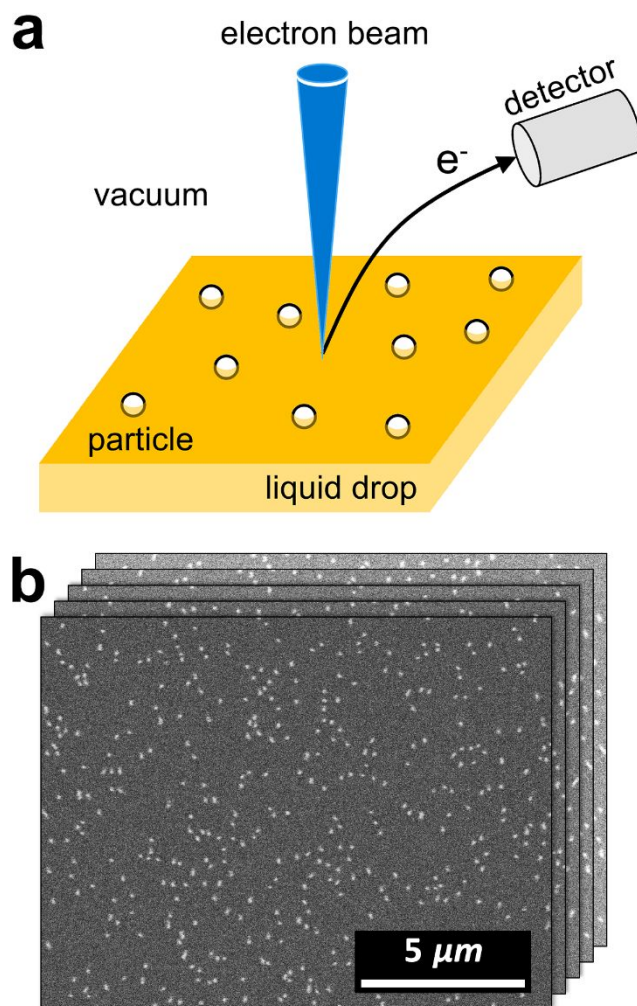


Figure 1. Schematic of imaging technique and SEM images of PEGylated NPs attached to vacuum-IL interfaces (a) Schematic of experimental setup. (b) SEM micrographs of 5 kDa PEGylated 200-nm silica NPs attached to IL surface. Each image covers $>250 \mu\text{m}^2$. 100~200 images were captured for the calculation of $g(r)$.

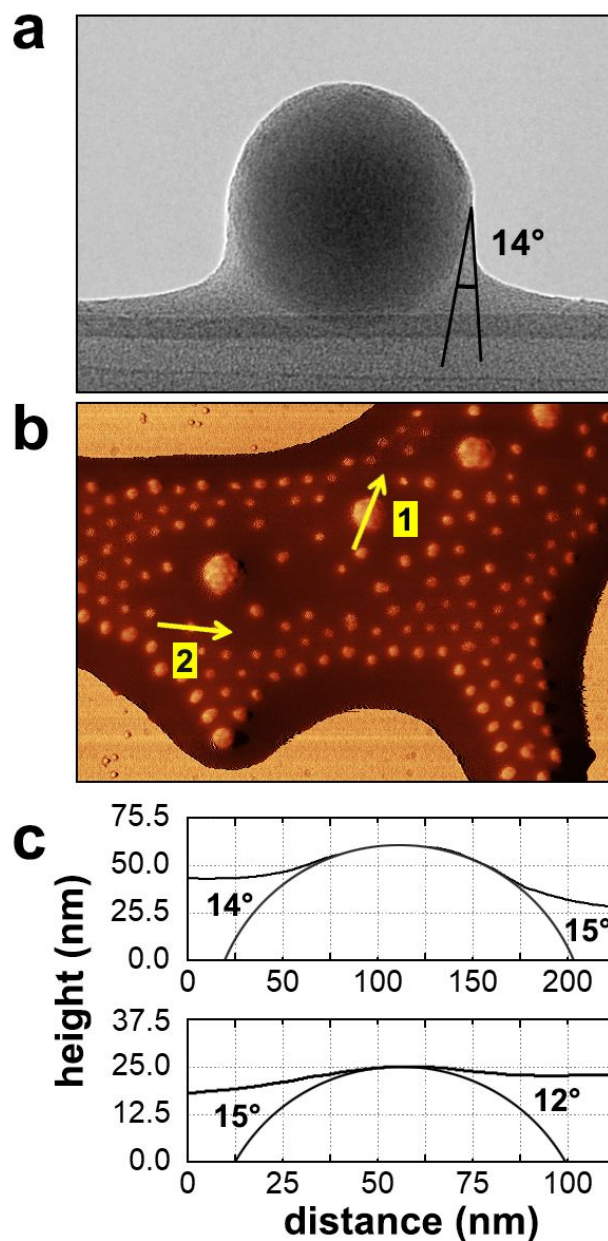


Figure 2. θ_c for NPs at vacuum (or air)-IL interfaces.

(a) TEM micrograph of a PEGylated 100-nm silica nanoparticle wetted (and pinned) by IL against the edge of an opening in lacey carbon. The image width is 170 nm. (b) AFM phase contrast image of a mixture of 100-nm and 200-nm silica NPs trapped by a thinner IL film against a planar solid substrate. The image width is 2.3 μm . (c) Height profiles near the contact line for 200-nm (top) and 100-nm (bottom) NPs along the arrows 1 and 2 indicated in (b). Each NP is fitted with a circle. NPs in (a), (b), and (c) are grafted with 5 kDa PEG.

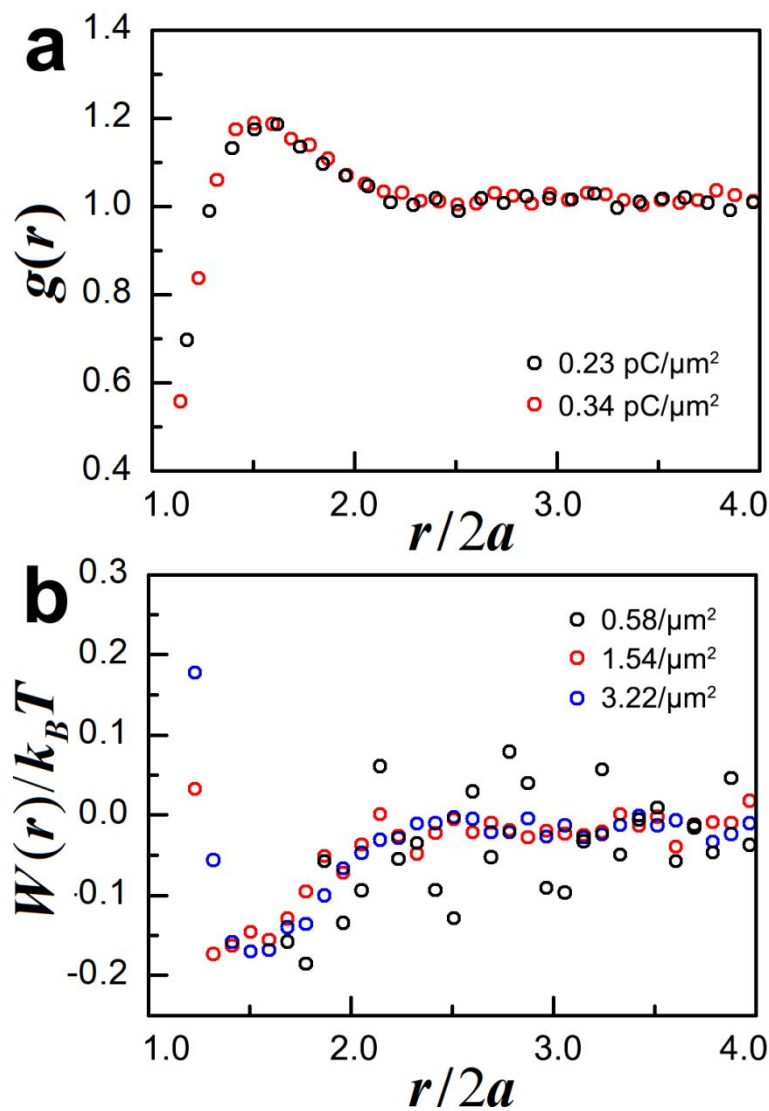


Figure 3. Effects of electron dose and NP areal number density on radial distribution function $g(r)$ and calculated potential of mean force $W(r)$. (a) $g(r)$ measured at two electron doses for a fixed areal number density of $1.54/\mu\text{m}^2$. (b) $W(r)$ measured at three low areal number densities for a fixed electron dose of $0.34 \text{ pC}/\mu\text{m}^2$. Both (a) and (b) are for 5 kDa PEGylated 200-nm silica NPs.

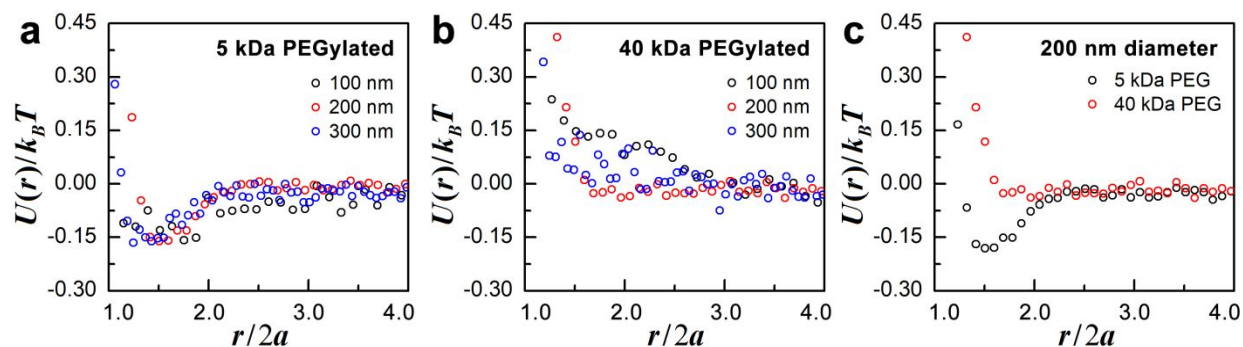
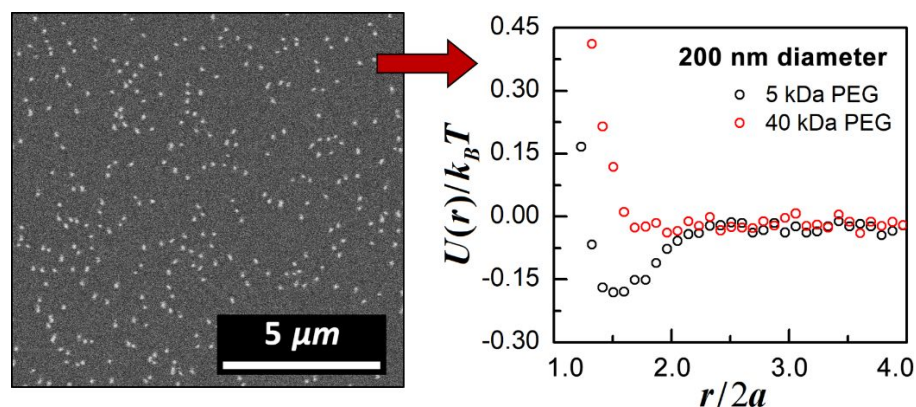


Figure 4. Pair interaction potential $U(r)$ for PEGylated silica NPs attached to IL surface. (a) $U(r)$ for 5 kDa PEGylated 100-, 200-, and 300-nm NPs. (b) $U(r)$ for 40 kDa PEGylated 100-, 200-, and 300-nm NPs. (c) $U(r)$ for 5 kDa and 40 kDa PEGylated 200-nm NPs compared.

TABLE OF CONTENTS (TOC)



REFERENCES

1. Bresme, F.; Oettel, M., Nanoparticles at Fluid Interfaces. *J. Phys.: Condens. Matter* **2007**, *19*, 413101.
2. Toor, A.; Feng, T.; Russell, T. P., Self-Assembly of Nanomaterials at Fluid Interfaces. *Eur. Phys. J. E* **2016**, *39*, 57.
3. Pieranski, P., Two-Dimensional Interfacial Colloidal Crystals. *Phys. Rev. Lett.* **1980**, *45*, 569-572.
4. Peng, Y.; Wang, Z.; Alsayed, A. M.; Yodh, A. G.; Han, Y., Melting of Colloidal Crystal Films. *Phys. Rev. Lett.* **2010**, *104*, 205703.
5. Bausch, A. R.; Bowick, M. J.; Cacciuto, A.; Dinsmore, A. D.; Hsu, M. F.; Nelson, D. R.; Nikolaidis, M. G.; Travesset, A.; Weitz, D. A., Grain Boundary Scars and Spherical Crystallography. *Science* **2003**, *299*, 1716-1718.
6. Binks, B. P.; Isa, L.; Tyowua, A. T., Direct Measurement of Contact Angles of Silica Particles in Relation to Double Inversion of Pickering Emulsions. *Langmuir* **2013**, *29*, 4923-4927.

7. Oettel, M.; Dietrich, S., Colloidal Interactions at Fluid Interfaces. *Langmuir* **2008**, *24*, 1425-1441.
8. Williams, D. F.; Berg, J. C., The Aggregation of Colloidal Particles at the Air—Water Interface. *J. Colloid Interface Sci.* **1992**, *152*, 218-229.
9. Girotto, M.; dos Santos, A. P.; Levin, Y., Interaction of Charged Colloidal Particles at the Air–Water Interface. *J. Phys. Chem. B* **2016**, *120*, 5817-5822.
10. Bresme, F.; Lehle, H.; Oettel, M., Solvent-Mediated Interactions between Nanoparticles at Fluid Interfaces. *J. Chem. Phys.* **2009**, *130*, 214711.
11. Hurd, A. J., The Electrostatic Interaction between Interfacial Colloidal Particles. *J. Phys. A: Math. Gen.* **1985**, *18*, L1055-L1060.
12. Levin, Y., Electrostatic Correlations: From Plasma to Biology. *Rep. Prog. Phys.* **2002**, *65*, 1577-1632.
13. Trizac, E.; Bocquet, L.; Aubouy, M., Simple Approach for Charge Renormalization in Highly Charged Macroions. *Phys. Rev. Lett.* **2002**, *89*, 248301.
14. Kralchevsky, P. A.; Nagayama, K., Capillary Interactions between Particles Bound to Interfaces, Liquid Films and Biomembranes. *Adv. Colloid Interface Sci.* **2000**, *85*, 145-192.
15. Nikolaidis, M. G.; Bausch, A. R.; Hsu, M. F.; Dinsmore, A. D.; Brenner, M. P.; Gay, C.; Weitz, D. A., Electric-Field-Induced Capillary Attraction between Like-Charged Particles at Liquid Interfaces. *Nature* **2002**, *420*, 299.
16. Foret, L.; Würger, A., Electric-Field Induced Capillary Interaction of Charged Particles at a Polar Interface. *Phys. Rev. Lett.* **2004**, *92*, 058302.
17. Lehle, H.; Oettel, M.; Dietrich, S., Effective Forces between Colloids at Interfaces Induced by Capillary Wavelike Fluctuations. *Europhys. Lett.* **2006**, *75*, 174-180.
18. Lehle, H.; Oettel, M., Stability and Interactions of Nanocolloids at Fluid Interfaces: Effects of Capillary Waves and Line Tensions. *J. Phys.: Condens. Matter* **2008**, *20*, 404224.
19. M. Gelbart, W.; P. Sear, R.; R. Heath, J.; Chaney, S., Array Formation in Nano-Colloids: Theory and Experiment in 2D. *Faraday Discuss.* **1999**, *112*, 299-307.
20. Sear, R. P.; Chung, S.-W.; Markovich, G.; Gelbart, W. M.; Heath, J. R., Spontaneous Patterning of Quantum Dots at the Air-Water Interface. *Phys. Rev. E* **1999**, *59*, R6255-R6258.
21. Butt, H.-J.; Cappella, B.; Kappl, M., Force Measurements with the Atomic Force Microscope: Technique, Interpretation and Applications. *Surf. Sci. Rep.* **2005**, *59*, 1-152.
22. Bevan, M. A.; Prieve, D. C., Direct Measurement of Retarded Van Der Waals Attraction. *Langmuir* **1999**, *15*, 7925-7936.
23. Israelachvili, J. N.; Adams, G. E., Measurement of Forces between Two Mica Surfaces in Aqueous Electrolyte Solutions in the Range 0–100 nm. *J. Chem. Soc., Faraday Trans. 1* **1978**, *74*, 975-1001.
24. Furst, E. M., Interactions, Structure, and Microscopic Response: Complex Fluid Rheology Using Laser Tweezers. *Soft Mater.* **2003**, *1*, 167-185.
25. Vondermassen, K.; Bongers, J.; Mueller, A.; Versmold, H., Brownian Motion: A Tool to Determine the Pair Potential between Colloid Particles. *Langmuir* **1994**, *10*, 1351-1353.
26. Iacovella, C. R.; Rogers, R. E.; Glotzer, S. C.; Solomon, M. J., Pair Interaction Potentials of Colloids by Extrapolation of Confocal Microscopy Measurements of Collective Suspension Structure. *J. Chem. Phys.* **2010**, *133*, 164903.
27. Chen, Q.; Cho, H.; Manthiram, K.; Yoshida, M.; Ye, X.; Alivisatos, A. P., Interaction Potentials of Anisotropic Nanocrystals from the Trajectory Sampling of Particle Motion Using *In Situ* Liquid Phase Transmission Electron Microscopy. *ACS Cent. Sci.* **2015**, *1*, 33-39.

- 1
2
3 28. Kim, P. Y.; Ribbe, A. E.; Russell, T. P.; Hoagland, D. A., Visualizing the Dynamics of
4 Nanoparticles in Liquids by Scanning Electron Microscopy. *ACS Nano* **2016**, *10*, 6257-6264.
- 5 29. Harner, J. M.; Hoagland, D. A., Thermoreversible Gelation of an Ionic Liquid by
6 Crystallization of a Dissolved Polymer. *J. Phys. Chem. B* **2010**, *114*, 3411-3418.
- 7 30. van Oss, C. J.; Chaudhury, M. K.; Good, R. J., Monopolar Surfaces. *Adv. Colloid Interface*
8 *Sci.* **1987**, *28*, 35-64.
- 9 31. Fröba, A. P.; Kremer, H.; Leipertz, A., Density, Refractive Index, Interfacial Tension, and
10 Viscosity of Ionic Liquids [Emim][Etso4], [Emim][Ntf2], [Emim][N(Cn)2], and [Oma][Ntf2] in
11 Dependence on Temperature at Atmospheric Pressure. *J. Phys. Chem. B* **2008**, *112*, 12420-12430.
- 12 32. Du, K.; Glogowski, E.; Emrick, T.; Russell, T. P.; Dinsmore, A. D., Adsorption Energy of
13 Nano- and Microparticles at Liquid-Liquid Interfaces. *Langmuir* **2010**, *26*, 12518-12522.
- 14 33. Cheung, D. L.; Bon, S. A. F., Interaction of Nanoparticles with Ideal Liquid-Liquid
15 Interfaces. *Phys. Rev. Lett.* **2009**, *102*, 066103.
- 16 34. Shkrob, I. A., Deprotonation and Oligomerization in Photo-, Radiolytically, and
17 Electrochemically Induced Redox Reactions in Hydrophobic Alkylalkylimidazolium Ionic
18 Liquids. *J. Phys. Chem. B* **2010**, *114*, 368-375.
- 19 35. Behar, D.; Gonzalez, C.; Neta, P., Reaction Kinetics in Ionic Liquids: Pulse Radiolysis
20 Studies of 1-Butyl-3-Methylimidazolium Salts. *J. Phys. Chem. A* **2001**, *105*, 7607-7614.
- 21 36. Egerton, R. F.; Li, P.; Malac, M., Radiation Damage in the TEM and SEM. *Micron* **2004**,
22 *35*, 399-409.
- 23 37. Kuwabata, S.; Kongkanand, A.; Oyamatsu, D.; Torimoto, T., Observation of Ionic Liquid
24 by Scanning Electron Microscope. *Chem. Lett.* **2006**, *35*, 600-601.
- 25 38. Ueno, K.; Inaba, A.; Kondoh, M.; Watanabe, M., Colloidal Stability of Bare and Polymer-
26 Grafted Silica Nanoparticles in Ionic Liquids. *Langmuir* **2008**, *24*, 5253-5259.
- 27 39. He, Z.; Alexandridis, P., Nanoparticles in Ionic Liquids: Interactions and Organization.
28 *Phys. Chem. Chem. Phys.* **2015**, *17*, 18238-18261.
- 29 40. Gebbie, M. A.; Smith, A. M.; Dobbs, H. A.; Lee, A. A.; Warr, G. G.; Banquy, X.; Valtiner,
30 M.; Rutland, M. W.; Israelachvili, J. N.; Perkin, S.; Atkin, R., Long Range Electrostatic Forces in
31 Ionic Liquids. *Chem. Commun.* **2017**, *53*, 1214-1224.
- 32 41. Gebbie, M. A.; Dobbs, H. A.; Valtiner, M.; Israelachvili, J. N., Long-Range Electrostatic
33 Screening in Ionic Liquids. *Proc. Natl. Acad. Sci. U. S. A.* **2015**, *112*, 7432-7437.
- 34 42. Ma, K.; Zhang, D.; Cong, Y.; Wiesner, U., Elucidating the Mechanism of Silica
35 Nanoparticle Pegylation Processes Using Fluorescence Correlation Spectroscopies. *Chem. Mater.*
36 **2016**, *28*, 1537-1545.
- 37 43. Smith, G. D.; Yoon, D. Y.; Jaffe, R. L.; Colby, R. H.; Krishnamoorti, R.; Fetters, L. J.,
38 Conformations and Structures of Poly(Oxyethylene) Melts from Molecular Dynamics Simulations
39 and Small-Angle Neutron Scattering Experiments. *Macromolecules* **1996**, *29*, 3462-3469.
- 40 44. Vasudevan, S. A.; Rauh, A.; Barbera, L.; Karg, M.; Isa, L., Stable in Bulk and Aggregating
41 at the Interface: Comparing Core-Shell Nanoparticles in Suspension and at Fluid Interfaces.
42 *Langmuir* **2018**, *34*, 886-895.
- 43 45. Scheidegger, L.; Fernández-Rodríguez, M. Á.; Geisel, K.; Zanini, M.; Elnathan, R.;
44 Richtering, W.; Isa, L., Compression and Deposition of Microgel Monolayers from Fluid
45 Interfaces: Particle Size Effects on Interface Microstructure and Nanolithography. *Phys. Chem.*
46 *Chem. Phys.* **2017**, *19*, 8671-8680.
- 47
48
49
50
51
52
53
54
55
56
57
58
59
60

- 1
2
3 46. Huang, S.; Gawlitza, K.; von Klitzing, R.; Gilson, L.; Nowak, J.; Odenbach, S.; Steffen,
4 W.; Auernhammer, G. K., Microgels at the Water/Oil Interface: *In Situ* Observation of Structural
5 Aging and Two-Dimensional Magnetic Bead Microrheology. *Langmuir* **2016**, *32*, 712-722.
6
7 47. Garbin, V.; Crocker, J. C.; Stebe, K. J., Nanoparticles at Fluid Interfaces: Exploiting
8 Capping Ligands to Control Adsorption, Stability and Dynamics. *J. Colloid Interface Sci.* **2012**,
9 *387*, 1-11.
10 48. Roerdink, J. B.; Meijster, A., The Watershed Transform: Definitions, Algorithms and
11 Parallelization Strategies. *Fundam. Inform.* **2000**, *41*, 187-228.
12 49. Hadjiiski, A.; Dimova, R.; Denkov, N. D.; Ivanov, I. B.; Borwankar, R., Film Trapping
13 Technique: Precise Method for Three-Phase Contact Angle Determination of Solid and Fluid
14 Particles of Micrometer Size. *Langmuir* **1996**, *12*, 6665-6675.
15
16
17
18
19
20
21
22
23
24
25
26
27
28
29
30
31
32
33
34
35
36
37
38
39
40
41
42
43
44
45
46
47
48
49
50
51
52
53
54
55
56
57
58
59
60